Understanding the coagulation mechanism and floc properties induced by Fe(VI) and $FeCl_3$: population balance modeling

Xinliang Liu, Hailiang Yin, Jian Zhao, Ziqi Guo, Zhen Liu and Yizhou Sang

ABSTRACT

Coagulation kinetics and floc properties are of great fundamental and practical importance in the field of water treatment. To investigate the performance of Fe(VI) and Fe(III) salt on particle coagulation, Malvern Mastersizer 2000 was employed to continuously and simultaneously monitor the kaolin floc size and structure change, and population balance modeling was used to investigate the coagulation mechanism. The results show dosage increase had positive effect on collision efficiency and floc strength and negative effect on restructure rate. Low shear rate resulted in higher collision efficiency and stronger floc. Low water temperature had a pronounced detrimental effect on coagulation kinetics. Temperature increase showed the most significant positive effect on collision efficiency, floc strength and restructure rate. The optimum pH zone for the coagulation was found to be between 6 and 8. Further pH increase lowered the collision efficiency and floc strength and increased the restructure rate. $FeCl_3$ resulted in a larger ratio of the mass to volume of kaolin flocs (compactness) than those induced by ferrate.

Key words | collision efficiency, ferric(III) chloride, floc strength, population balance model, potassium ferrate(VI), restructure rate

Xinliang Liu
Hailiang Yin
Jian Zhao
Ziqi Guo
Zhen Liu
Yizhou Sang (corresponding author)
Academy of Science and Technology,
China University of Petroleum,
Qingdao, Shandong Province 266555,
China
E-mail: *yzsang@gmail.com*

Yizhou Sang
National University Science Park,
China University of Petroleum,
Dongying, Shandong Province 207062
and
College of Chemical Engineering,
China University of Petroleum,
Qingdao, Shandong Province 266555,
China

HIGHLIGHTS

- Population balance modeling achieved excellent approximation of coagulation process.
- $FeCl_3$ produced larger, stronger and more compact flocs than those by ferrate(VI).
- Dosage increase had positive effect on collision efficiency and floc strength.
- High temperature resulted in high collision efficiency, floc strength and restructure.
- Optimum pH for both coagulation systems was between 6 and 8.

doi: 10.2166/wst.2021.150

GRAPHICAL ABSTRACT

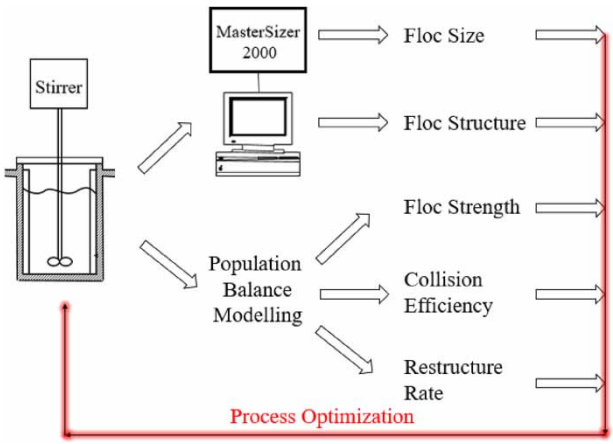

INTRODUCTION

As a result of self-decay and/or reactions with reductants (Zhou *et al.* 2019), ferrate(VI) (i.e. FeO_4^{2-}) eventually becomes stable ferric ions (Fe(III)) via more active intermediate high valence iron species (i.e. Fe(V) and Fe(IV)) through electron flow. It is thus considered as a multifunctional water treatment agent due to its ability to oxidize, disinfect and coagulate simultaneously the undesirable substance in the water (Sharma *et al.* 2015). While most of the publication available focused on the oxidation functionality of Fe(VI) (Graham *et al.* 2010), only few studies have been conducted to evaluate its coagulation performance of Fe(VI) in water because it is hard to separate the coagulation effects from its multifunctionalities (Yu *et al.* 2016). Though the aforementioned difficulties, few efforts were still made to investigate the mechanisms of Fe(VI) coagulation along with its performance in the removal of colloidal particles from water. However, the results are inconsistent. Fe(VI) was reported as a better coagulant than Fe(III) when it was used to treat upland colored water (Jiang *et al.* 2001). Better algae and turbidity removal was observed when Fe(VI) was used as a pre-oxidation agent before alum coagulation (Ma & Liu 2002a, 2002b). It is reported Ferrate(VI) achieved comparable, or better, floc formation to ferric chloride, but less dissolved organic carbon (DOC) removal in humic acid solution in the absence of particulate matter (Graham *et al.* 2010). Fe(VI) pre-oxidation also improved the effluent turbidity of a downstream dual-media filter in continuous flow treatment experiments (Goodwill *et al.* 2016). In contrast, some research showed that Fe(III) demonstrated better coagulation effect than Fe(VI) using photometric dispersion analyzer 2000 (PDA 2000, Rank Brother, Inc., Cambridge, UK) (Yu *et al.* 2016). The flocs resulted from Fe(VI) and Fe(III) effects were different in size distributions and morphologies. Moreover, Fe(VI) resultant particles were mainly composed of crystalline Fe_2O_3, which was not detected in the Fe(III) resultant particles, as well as more nanoparticles that generated a stable colloidal suspension (Goodwill *et al.* 2015). It was found that the majority of Fe(VI)-induced flocs was suspended in the secondary effluent indicating its poor settleability (Zheng & Deng 2016). Fe(VI) dose played a key role in the size distribution and coagulation (Cui *et al.* 2018). High Fe(VI) dose could accelerate the aggregation of fine particles and facilitate downstream solid-liquid separation.

In order to only evaluate the coagulation ability of ferrate and clarify the coagulation performance of ferrate and Fe(III) salt, kaolin was used as the modelled solid particle in water suspension since it is inert to the oxidation effect of ferrate, so the observations of particle growth are believed to be caused by the coagulation effects of ferrate hydrolysis species and the $FeCl_3$ (Tien *et al.* 2008).

It is commonly admitted that floc properties (such as floc size, structure and strength) of Fe(VI) and $FeCl_3$ induced flocs have significant effect on the solid-liquid separation (Sang & Xiao 2008, 2009; Sang & Englezos 2012). Large and compact floc would facilitate the sedimentation and solid-liquid separation (Hubbe 2005). Previously, either jar test or photometric dispersion analyzer were employed

to evaluate such floc properties. However, both methods have limitations. Conventional jar test methods are limited in terms of sensitivity and practical convenience, though they do provide a useful visual and semi-quantitative simulation of Fe(VI) and $FeCl_3$ induced coagulation (Lv *et al.* 2018). Photometric dispersion analyzer (Rank Brother, Inc., Cambridge, UK), based on optical technique, can provide sensitive and rapid response of Fe(VI) and $FeCl_3$ induced coagulation. However, information about degree of coagulation and the strength of flocs is 'relative'. The degree of coagulation/flocculation is represented by a 'relative' turbidity. The floc strength is expressed as strength factor which is determined by the ratio of 'relative' turbidity obtained before and after the sudden increase in shear rate (Tien *et al.* 2008). Both aforementioned methods did not provide information on the real floc size, structure and strength. Traditionally, floc structure is assessed by microscopy imaging or transmission electron microscope (TEM) (Lv *et al.* 2018). The result is not representative for all the floc presented in the suspension as this method is limited to the measurement of only a few hundred flocs. It is time consuming and requires the performance of highly demanding procedures due to the fragility of the flocs.

It is thus necessary to take advantage of the latest developed technology which can monitor the floc properties during Fe(VI) and $FeCl_3$ induced coagulation (Benn *et al.* 2018; Chassagne & Safar 2020). Mass fractal dimension is such a concept which describes the floc structure and the dynamic light scattering technique makes its measurement possible (Callesen *et al.* 2018). Therefore, the first objective of this research was to continuously monitor the floc size and floc structure change through dynamic light scattering using Mastersizer 2000 (Malvern Instruments Inc., Malvern, UK).

Strong flocs are desirable for solid-liquid separation during water treatment as good strength minimizes the floc breakage and increases the removal efficiency. The higher the floc density, the stronger the floc, the easier the removal of particles (Gregory 2004). Floc strength is therefore used to assess the floc quality. A traditional floc strength characterization is carried out by observing the floc index response to a sudden shear rate increase within a Gator reactor (Smith & Kitchener 1978). In order to measure the floc strength, micromechanical technique was developed to rupture a single floc in the tensile mode (Yeung & Pelton 1996). Because of limited measurement of flocs and highly demanding procedure due to floc fragility, micromechanical technique cannot provide the representative result for floc strength.

In order to manipulate the floc properties during Fe(VI) and $FeCl_3$ induced coagulation, there is a need to obtain the quantitative information of floc strength and its dependence on process parameters. It is known floc breakup would happen when the hydrodynamic force applied to the flocs is equal or greater than the floc strength (Rau *et al.* 2018). Through incorporating the breakage rate and the critical energy dissipation rate required for the floc breakage into the population balance model, floc strength can be extracted. This is the second objective of this research.

In order to assist the judicial selection of chemicals and optimization of operating parameters, it is desired to have the relationship between collision efficiency, restructure rate and process conditions. Establishment of such relationship is the third objective of this research.

MATERIALS AND METHODS

Materials

Kaolin, obtained from Chenming Group, China, was used as the model suspended solid in the water. The inherent volumetric mean particle size of the kaolin is 2.79 μm as measured by Mastersizer 2000 (Malvern Instruments Inc., Malvern, UK). It has a wide size distribution with the lowest limit size of 0.24 μm and the largest limit size of 7.26 μm. Kaolin suspension (50 mg/L) was prepared by adding kaolin to deionised distilled water and mixing thoroughly. $FeCl_3$ and K_2FeO_4, both analytical regents, obtained from Chenming Group, China. Ferric chloride stock solution at a concentration of 0.01 mol/L was prepared by dissolving 2.71 g $FeCl_3.6H_2O$ in 1 L deionised and distilled water immediately before the tests. Boric acid/NaOH (pH 9.0) buffer solution, prepared by mixing 50 mL 0.1 M boric acid/0.1 M KCl solution, 20 mL 0.1 M NaOH solution and 30 mL distilled and deionised water, was used to make ferrate solution. To maintain the reactivity of ferrate, stock K_2FeO_4 solutions were prepared immediately before use. Bicarbonate buffer solution (0.2 M) was made by dissolving NaHCO3 (Chenming Group, China) in distilled and deionised water. HCl and NaOH, analytical grade, were used to control pH values of the coagulation system.

Coagulation experiment

The kaolin coagulation process was continuously monitored by Mastersizer 2000 (Malvern Instruments Inc., Malvern, UK) where a peristaltic pump was used to circulate the

kaolin suspension (50 mg/L) to the instrument for particle size and structure characterization. Figure 1 shows the schematic of the kaolin coagulation setup. Water bath was used to control the experiment temperatures. pH of the coagulation system was controlled by the addition of HCl and NaOH. The temperature, shear rate, pH, dosages of Fe(VI) and $FeCl_3$ were adjusted accordingly to investigate their effects on the coagulation process. Kaolin is assumed to be inert to the oxidation effect of the ferrate and thus the observed floc properties (e.g. floc size, structure and strength) change could be regarded as the coagulation effects of Fe(III) from Fe(VI) self-decomposition. Experiments were conducted in the normal pH range of surface water and groundwater of 6 to 10.

Mass fractal dimension

Mass fractal dimension of flocs was calculated by Equation (1) from the scattered light density information obtained from Malvern Mastersizer 2000 (Teixeira 1988):

$$Q = \frac{\pi n \sin(\theta/2)}{\lambda} \tag{1}$$

where n is the fluid refractive index, λ is the laser light wavelength in vacuum, and θ is the scattering angle. The mass fractal dimension was obtained from the negative slope of the linear region of the log-log plot of scattered light intensity I(q) versus scattering vector Q (Bushell *et al.* 2002).

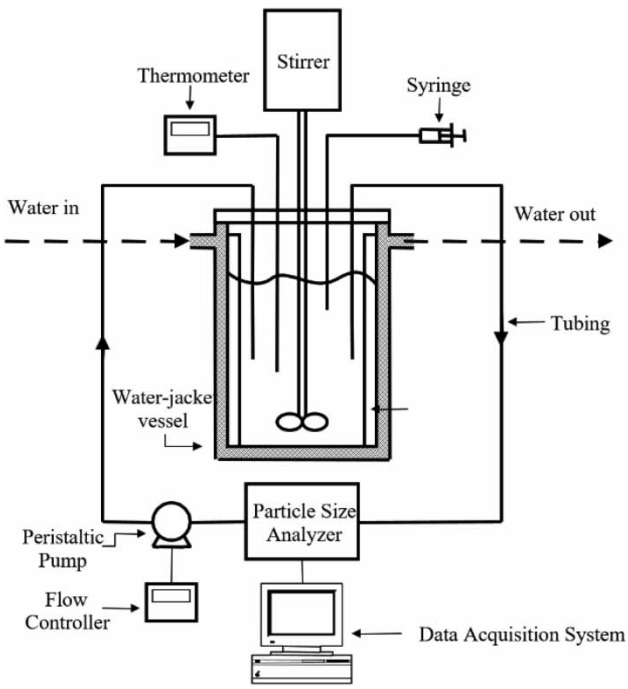

Figure 1 | Schematic of kaolin coagulation setup.

Population balance model

By discretizing the population balance model originally proposed by Smoluchowski (von Smoluchowski 1917) with respect to size and converting it to a set of nonlinear ordinary differential equations (ODE), the particle number concentration change rate in section i used for corresponding particle size calculation is given by (Hounslow *et al.* 1988):

$$\begin{aligned}\frac{dN_i}{dt} = {} & N_{i-1}\sum_{j=1}^{i-2} 2^{j-i+1}\alpha_{i-1,j}\beta_{i-1,j}N_j + \frac{1}{2}\alpha_{i-1,i-1}\beta_{i-1,i-1}N_{i-1}^2 \\ & - N_i\sum_{j=1}^{i-1} 2^{j-1}\alpha_{i,j}\beta_{i,j}N_j - N_i\sum_{j=i}^{i\max}\alpha_{i,j}\beta_{i,j}N_j \\ & - S_iN_i + \sum_{j=i}^{i\max}\Gamma_{i,j}S_jN_j \end{aligned} \tag{2}$$

where N_i is the number concentration of particles in section i, $\alpha_{i,j}$ is the collision efficiency, and $\beta_{i,j}$ is the collision frequency for the particles in sections i and j. The number concentration of primary particles is used as the initial condition for the population balance equation. Fragmentation rate S_j was used to describe the floc breakage rate. The distribution of floc fragments in interval i from the break-up of flocs in interval j was described by the breakage distribution function Γ_{ij}. The first two terms on the right hand side of Equation (2) represent the aggregation birth of floc of size, i. The third and fourth terms represent the death of floc of size, i, due to aggregation. The fifth term is the death of floc of size, i. The sixth term is the breakage birth of floc of size, i, by breakage of larger flocs in interval j.

Collision efficiency

Collision efficiency is modeled either as a fitting parameter or as a function of the interaction forces between particles which take into account bridging attraction or steric repulsion, van der Waals attraction and electrical double layer repulsion between particles (Runkana *et al.* 2006). However, calculation of hydrodynamic interactions and short-range forces is required to determine the collision efficiency. Colloidal interactions and hydrodynamic retardation effects are usually ignored in the rectilinear model and then the collision efficiency is overestimated. Experimental data does not support the collision efficiency calculated by curvilinear

model using DLVO theory (Wiesner 1992). Thus, a shell-core model was developed which enables a more accurate prediction of collision efficiency for the growth of floc (Kusters 1991). Due to its accuracy, it is adopted as a fitting parameter for population balance equation in this research and is described by Equation (3) (Kusters 1991).

$$\alpha_{i,j} = \frac{\exp\left(-0.1(1-(i/j))\right)^2}{(i\times j)^{0.1}} \times \alpha_{\max} = \frac{\exp\left(-0.1(1-(i/j))\right)^2}{(i\times j)^{0.1}} \quad (3)$$

where, i and j represent the discretized sections of the floc size distribution. α_{max}, the maximum collision efficiency, equals to unity.

Collision frequency

The collision frequency, determined by particle radius, is defined as the number of particles passing through the capture cross-section per unit time. For particles smaller than one micron (Liu *et al.* 2012), the collision frequency is mainly determined by the Brownian motion if settling and inertial phenomenon are ignored (Hsu *et al.* 2001).

Equation (4) gives the collision frequency of particles smaller than one micron due to Brownian motion (Saffman & Turner 1956):

$$\beta_{ij,perikinetic} = \left(\frac{2k_BT}{3\mu}\right)\frac{(R_{ci}+R_{cj})^2}{R_{ci}R_{cj}} \quad (4)$$

where k_B is the Boltzmann constant, T is the absolute temperature, and μ is the dynamic viscosity. R_{ci} and R_{cj} are the collision radius, which can be calculated from the primary particle radius r_0, the total number N of primary particles of the flocs in section i and the mass fractal dimensions d_f of the flocs (Saffman & Turner 1956):

$$R_{Ci} = r_0 N^{1/d_f} \quad (5)$$

On the other hand, fluid motion and orthokinetic collision dominate the collision of particles larger than one micron. Both particle size and shear rate determine such collision frequency (Elimelech *et al.* 1995). The collision frequency of orthokinetic collisions between particles in sections i and j is calculated by Equation (6) (Elimelech *et al.* 1995).

$$\beta_{ij,orthokinetic} = 1.3\sqrt{\varepsilon/\nu}(R_{ci}+R_{cj})^3 \quad (6)$$

where ε (m^2/s^3) is the average energy dissipation rate, υ is the kinematic viscosity (m^2/s). It shows the collision frequency is proportional to the cube of the particle radius, which has the major effect on the floc growth rate. The larger the floc size, the bigger the collision frequency.

Summing the collision caused by the perikinetic and orthokinetic motion, overall collision frequency is shown in Equation (7).

$$\beta_{ij} = \beta_{ij,perikinetic} + \beta_{ij,orthokinetic} \quad (7)$$

Relationship between energy dissipation rate and breakage rate

The shear rate, flocs porosity, floc size and floc strength affect the breakability of the floc. Floc breakup happens when hydrodynamic force applied to the flocs is equal or greater than the aggregate strength (Kusters 1991). Equation (8) shows the relationship between the breakage rate S_i and the critical energy dissipation rate required for the floc breakage (Kusters 1991):

$$S_i = \left(\frac{4}{15\pi}\right)^{1/2}\left(\frac{\varepsilon}{\nu}\right)^{1/2}\exp\left(\frac{-\varepsilon_{ci}}{\varepsilon}\right) \quad (8)$$

where ε_{ci} is the critical energy dissipation rate per unit mass of fluid which cause the floc breakup, $J\cdot s^{-1}\cdot kg^{-1}$ (Shirazi *et al.* 2003).

Breakage distribution function

Binary breakage, ternary breakage and normally distributed breakage are the three most possible breakage distribution during the floc breakage process. Binary breakage functions resulted in sufficiently accurate and simple implementation compared to ternary breakage and normally distributed breakage functions (Spicer & Pratsinis 1996). Thus, the binary breakage distribution function shown in Equation (9) was chosen for modeling.

$$\Gamma_{ij} = \frac{V_j}{V_i} = 2 \text{ for } j = i+1 \qquad \Gamma_{ij} = 0 \text{ for } j \neq i+1 \quad (9)$$

By using the information of number concentration N_i of the particles in all the intervals and the characteristic floc diameter (m) in interval i (Kusters 1991), the volume mean

diameter $d_{4,3}$ (m) was calculated as in Equation (10):

$$d_{4,3} = \Sigma N_i D_i^4 / \Sigma N_i D_i^3 \quad (10)$$

where, characteristic floc diameter (m) in interval i is calculated by the d_0 and d_f obtained from Malvern Mastersizer 2000 measurement

$$D_i = (2^{(i-1)/d_f}) d_0 \quad (11)$$

Floc structure change rate characterization

The floc structure changed during the coagulation process and its change rate can be represented by the dynamic change of mass fractal dimension and the rate can be calculated by Equation (12) (Bonanomi *et al.* 2004):

$$\frac{dd_f}{dt} = \gamma(d_{f,\max} - d_f) \quad (12)$$

γ (s^{-1}) is restructure rate as fitting parameter and $d_{f,\max}$ is the maximum mass fractal dimension value.

Parameter estimation

Objective function with collision efficiency α, critical energy dissipation rate ε_{ci}, and restructure rate γ as variables to be minimized is shown in Equation (13). Fminsearch solver in Matlab which uses Nelder-Mead simplex algorithm was used to find the minimum of the least squares:

$$f(\alpha, \varepsilon_{ci}, \gamma) = \sum_{t=0}^{t=t_{\max}} (d_{4,3\text{expt}} - d_{4,3\text{model}})^2 \quad (13)$$

Ratio of the mass to volume of settled kaolin flocs (compactness)

The ratio of the mass to volume of settled kaolin flocs (compactness) was calculated as the ratio of the mass to the volume of settled flocs after 30 min of settling experiments.

RESULTS AND DISCUSSION

Kaolin coagulation: experiment and simulation

As shown in Figure 2, population balance modeling achieved excellent approximation of kaolin floc size and floc structure

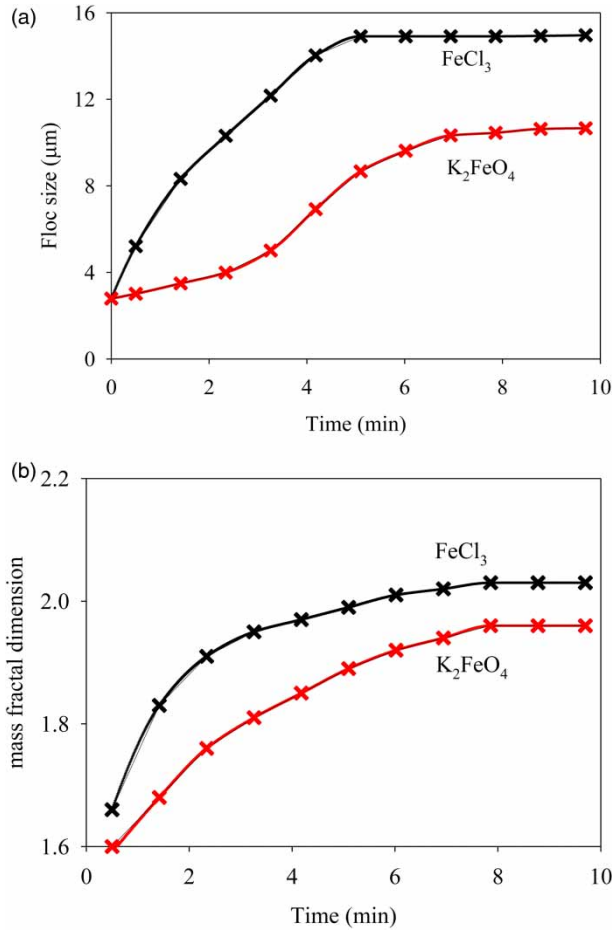

Figure 2 | Experimental and simulated kaolin coagulation induced by K_2FeO_4 and $FeCl_3$. (a) coagulation kinetics; (b) mass fractal dimension. Experimental conditions: dosage of Fe(VI) and $FeCl_3$ = 150 μM, pH = 7; shear rate = 50 s^{-1}; temperature = 25 °C. Notes: the data point is the experimental results whereas the connecting line shows the simulation result.

change induced by the K_2FeO_4 and $FeCl_3$ systems. The time required to reach steady state was about 8 min for K_2FeO_4 system and 5 min for $FeCl_3$ system. The observed substantial floc formation induced by the two chemicals at iron concentration of 150 μM and neutral pH is corresponding to the sweep flocculation mechanism where kaolin is enmeshed within amorphous ferric hydroxide precipitates.

The results confirmed the simultaneous occurrence of aggregation, breakage and restructure during the coagulation process. During the initial stage of the coagulation, aggregation is the dominated factor which governs the floc growth. Meanwhile, floc became more susceptible to the hydrodynamic shear which broke, compacted (restructure effect) and limited the further growth of floc. It is evident that ferric chloride demonstrated better performance over potassium ferrate in inducing kaolin coagulation. This is probably because (1) the slow ferrate decomposition for

coagulation and (2) the decomposition of Fe(VI) yields nanoparticles having a core-shell nanoarchitecture with a γ-Fe_2O_3 core and a γ-FeOOH shell (Prucek *et al.* 2013), which has a lower coagulation ability (Yu *et al.* 2016). Ferric chloride produced more compact flocs than those produced by potassium ferrate, as indicated by the higher mass fractal dimension. The mass fractal dimension also increased as coagulation proceeded, suggesting more compact flocs were formed.

Effect of dosage of potassium ferrate(VI) and $FeCl_3$ on collision efficiency, energy dissipation rate and restructure rate

Figure 3 shows the positive effect of potassium ferrate(VI) and $FeCl_3$ dosage increase on collision efficiency and floc strength (indicated by energy dissipation rate) and negative effect on restructure rate. Increasing the coagulant dosage gives progressively larger and stronger flocs but, little further improvement was observed beyond the optimum dosage.

Compared to potassium ferrate(VI) system, $FeCl_3$ system demonstrated higher collision efficiency, higher floc strength and lower restructure rate. The inferior performance of ferrate system in comparison to ferric chloride is due to the slow decomposition of ferrate in water and low activity of the resulted iron nanoparticle for coagulation (Yu *et al.* 2016). The increase of potassium ferrate(VI) dosage would result in more decomposed iron nanoparticle for kaolin coagulation and thus higher collision efficiency. At the same time, high dosage provided more open structure from hydroxide precipitates for capturing colloidal particles and thus increased the collision efficiency and produced stronger flocs (Tran Tien 2012). It is also possible that the 'bridging" of particles by precipitated hydroxide may give stronger aggregates.

Increasing Fe(VI) and $FeCl_3$ dosage resulted in larger and stronger floc as indicated by the higher energy dissipation rate and lower restructure rate at high dosage. Compared to Fe(VI) system, higher energy dissipation rate (Figure 3(b)) and lower restructure rate (Figure 3(c)) of $FeCl_3$ coagulation system is due to the larger and more compact flocs produce by the system, as shown in Figure 2.

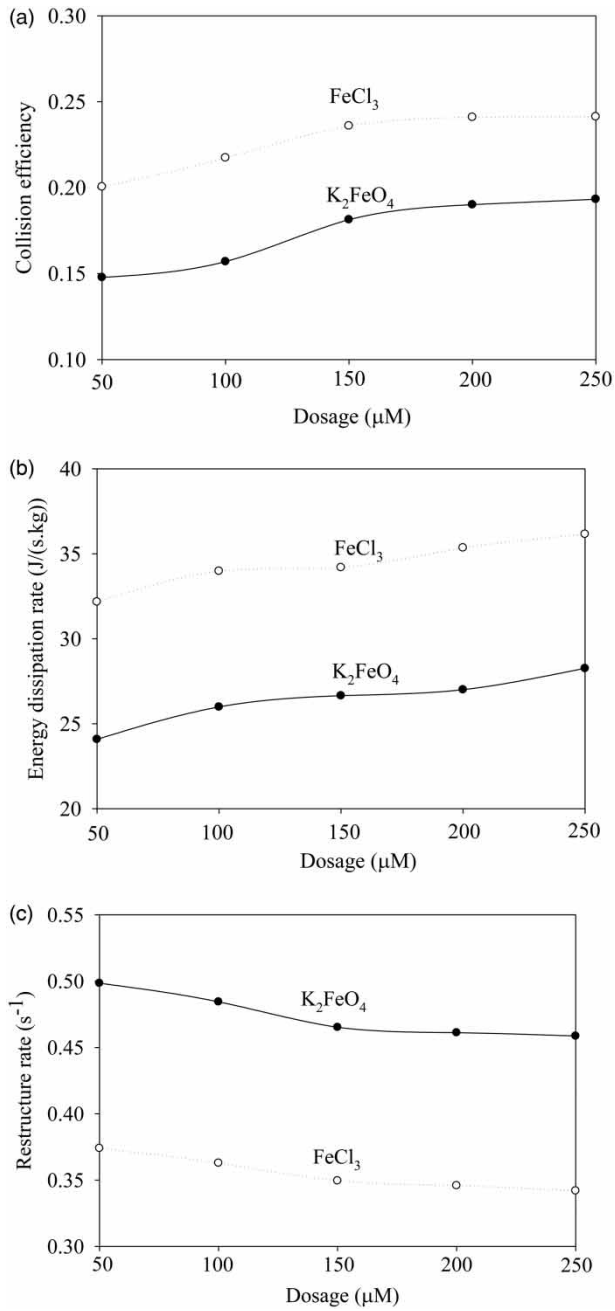

Figure 3 | Potassium ferrate(VI) and $FeCl_3$ dosage effect on (a) collision efficiency, (b) energy dissipation rate and (c) restructure rate. Experimental conditions: pH = 7; shear rate = 50 s^{-1}; temperature = 25 °C.

Effect of shear rate on collision efficiency, energy dissipation rate and restructure rate

Figure 4 shows $FeCl_3$ system resulted in higher collision efficiency, stronger floc and lower restructure rate than Fe(VI) system over the whole range of shear rate investigated. As shown in Figure 4(a) and 4(b), shear rate had a profoundly negative effect on collision efficiency and floc strength for both systems. Collision efficiency was lowered at high shear rate probably because the open structure and the bridge formed by hydroxide precipitates for colloidal particle capture were broken and therefore bonding point between the particles was reduced (Tran Tien 2012). Because of the reduction of bonding point, weaker floc was formed.

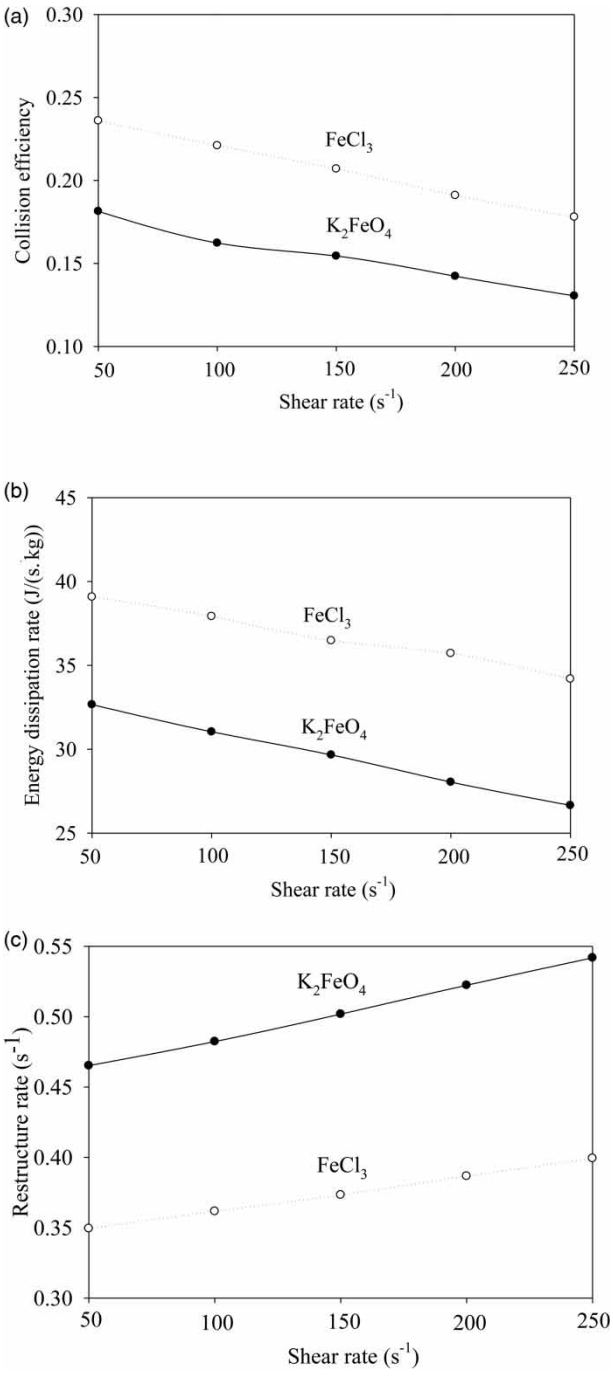

Figure 4 | Effect of shear rate on (a) collision efficiency, (b) energy dissipation rate and (c) restructure rate. Experimental conditions: dosage of ferrate(VI) and $FeCl_3$ = 150 μM; pH = 7; temperature = 25 °C.

Restructure rate increase with the increase of shear rate was observed for both coagulants as shown in Figure 4(c). As the increase of shear rate, more force was applied to the flocs and thus more significant restructure. Restructure processes would help particles to rearrange their position within the flocs and form additional bonds to densify the flocs.

Effect of temperature on collision efficiency, energy dissipation rate and restructure rate

Figure 5 shows temperature increase positively affected the collision efficiency, floc strength and restructure rate. This phenomenon may be explained by the temperature effects on the particle transport processes and the

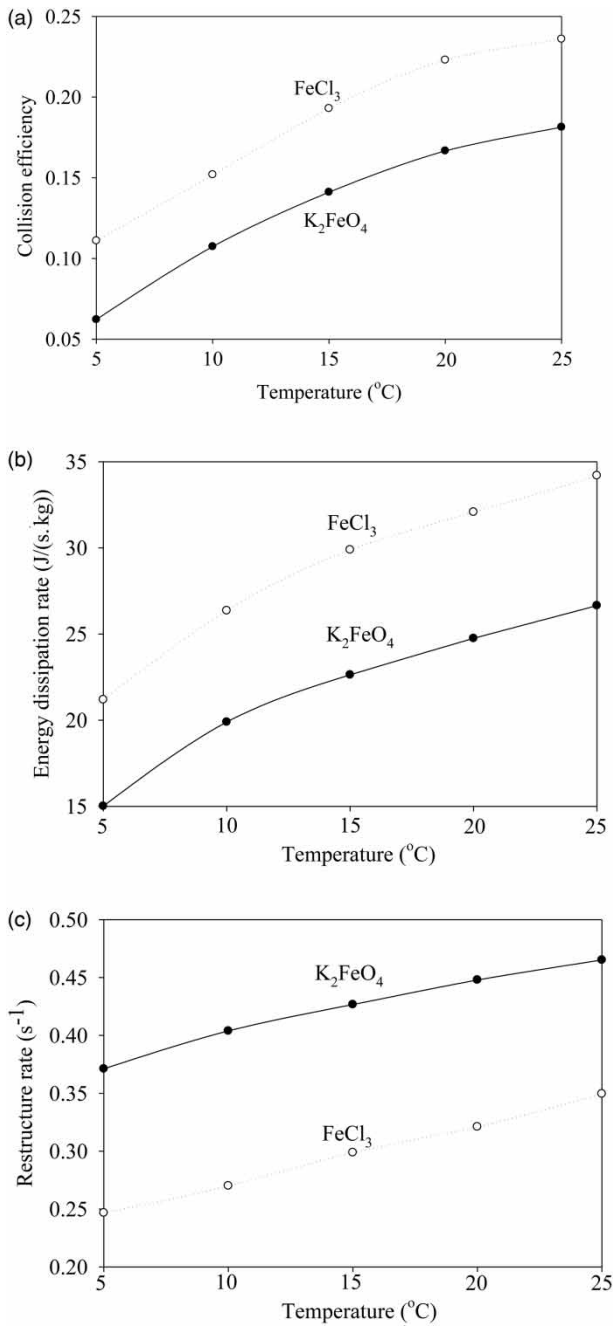

Figure 5 | Effect of temperature on (a) collision efficiency, (b) energy dissipation rate and (c) restructure rate. Experimental conditions: dosage of ferrate(VI) and $FeCl_3$ = 150 μM; pH = 7; shear rate = 50 s^{-1}.

coagulant chemistry. Through its effect on viscosity, and therefore on the mixing energy dissipated in water, water temperature eventually affects the particle collision rates during coagulation. Low temperature would negatively affect the fluid-particle interaction, particle-particle interaction, rate and extent of hydrolysis of metal salt coagulants, and adsorption and precipitation rates (Duan & Gregory 2003). For particles with a size greater than approximately 1 μm, orthokinetic collision dominates the coagulation process. However, orthokinetic collision caused by fluid shear diminished as the viscosity increased with decreasing temperature (Vik & Eikebrokk 1989). The poor rapid-mixing conditions at low water temperature also led to inhomogeneous coagulant distribution and resulted in poor coagulation (Vik & Eikebrokk 1989). Temperature decrease negatively affected the hydrolysis of ferrate(VI) and $FeCl_3$ and the precipitation and solubility of $Fe(OH)_3$ (Duan & Gregory 2003). High collision efficiency observed as temperature increase can be reasonably attributed to the effect of temperature on the perikinetic and orthokinetic aggregation process. High temperature has a positive effect on perikinetic collision frequency and results in more rapid Brownian motion as shown by Equation (4). Meanwhile, temperature increase also reduced the viscosity of water and facilitated fluid-particle interaction and particle-particle interaction and thus the coagulation process. Meanwhile, low viscosity of the system at high temperature would allow the shear force much easier to be transferred to flocs and restructure them. That is the possible reason for the high restructure rate observed at high temperature.

Effect of pH on collision efficiency, energy dissipation rate and restructure rate

Figure 6 shows the optimum pH for both coagulation system is between 6 and 8 where higher collision efficiency and stronger flocs were observed. It is well established the decomposition rate of ferrate depends on pH (Li *et al.* 2005). In order to achieve better Fe(VI) coagulation performance, it is desired to have higher Fe(VI) decomposition rate to generate Fe(III) for coagulation and lower solubility of amorphous iron(III) hydroxide to capture the colloidal particle. Fe(VI) has highest decomposition rate (Li *et al.* 2005) and lowest solubility of amorphous iron(III) hydroxide over pH range of 6 to 8 (Amirtharajah & Melia 1990; Tran Tien 2012). Fe(III) has limited solubility at pH range of 6 to 8 and the amorphous hydroxide would enmesh colloidal particles and cause hetero-coagulation (Duan & Gregory 2003). The combination of high Fe(VI) decomposition rate and low $Fe(OH)_3$ solubility at pH range of 6 to 8 made the collision efficiency high and floc strong.

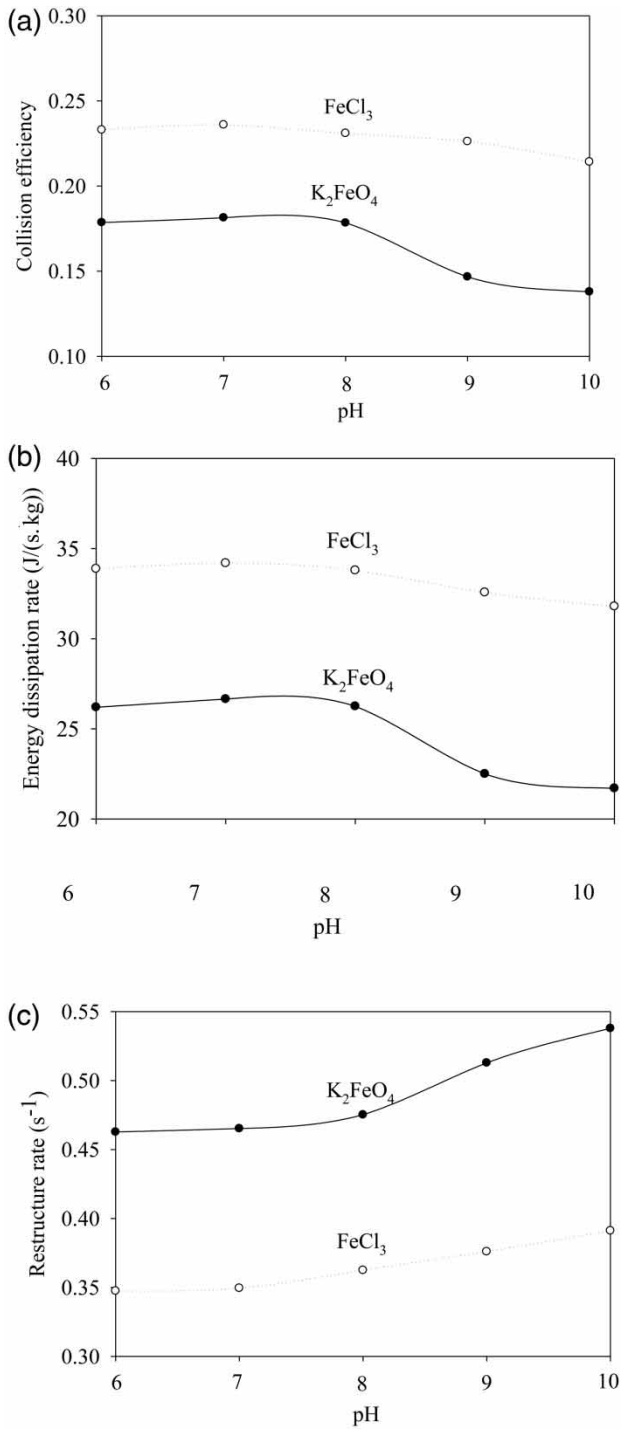

Figure 6 | Effect of pH on (a) collision efficiency, (b) energy dissipation rate and (c) restructure rate. Experimental conditions: dosage of ferrate(VI) and $FeCl_3$ = 150 μM; shear rate = 50 s^{-1}; temperature = 25 °C.

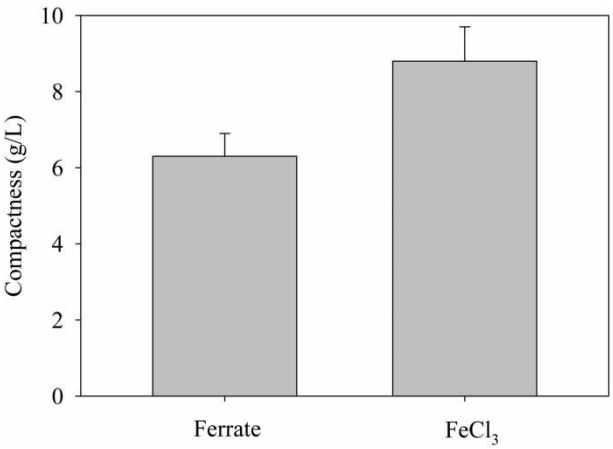

Figure 7 | Ratio of the mass to volume of settled kaolin flocs (compactness). Experimental conditions: dosage of ferrate(VI) and $FeCl_3$ = 150 μM; pH = 7; shear rate = 50 s^{-1}; temperature = 25 °C.

More significant decrease of collision efficiency and floc strength was observed for ferrate system than $FeCl_3$ system when pH was increased beyond 8. This is probably because, at this pH range, Fe(VI) became extremely stable and had very low (close to zero) decomposition rate (Li *et al.* 2005). It is reported minimum decomposition rate was observed between pH 9.2 and 9.4 that means almost no Fe(III) was produced for coagulation (Li *et al.* 2005). Meanwhile, pH increase also decreased the positive charge of the amorphous iron(III) hydroxide and increased its solubility which made it less effective to induce coagulation (Tran Tien 2012). The more significant restructure observed at high pH is most likely due to the low strength flocs produced which made them more susceptible to restructure.

Ratio of the mass to volume of settled kaolin flocs (compactness)

Figure 7 shows the ratio of the mass to volume of settled kaolin flocs (compactness) after addition of ferrate or $FeCl_3$. As shown in the figure, $FeCl_3$ resulted in a larger ratio of the mass to volume of kaolin flocs (compactness) than those induced by ferrate. This result further confirmed more compact flocs formed by $FeCl_3$ as indicated by larger mass fractal dimension shown in Figure 2. More compact floc would facilitate the particle separation from water suspension through sedimentation process (Wilen *et al.* 2003). Meanwhile, the formation of more compact floc could expel water from flocs which can also facilitate drainage during compressing (Hubbe 2005). The difference in the compactness is probably because the core-shell nanoarchitecture with a γ-Fe_2O_3 core and a γ-FeOOH shell from Fe(VI) decomposition has a lower coagulation ability than $FeCl_3$ (Yu *et al.* 2016).

CONCLUSIONS

Population balance modeling achieved excellent approximation of kaolin floc size evolution induced by Fe(VI) and $FeCl_3$. Ferric chloride produced larger, stronger and more compact flocs than those produced by potassium ferrate. Potassium ferrate(VI) and $FeCl_3$ dosage increase had positive effect on collision efficiency and floc strength and negative effect on restructure rate. $FeCl_3$ system resulted in higher collision efficiency, stronger flocs and lower restructure rate than Fe(VI) system over the whole range of shear rate investigated. Temperature increase positively affected the collision efficiency, floc strength and restructure rate. Optimum pH for both coagulation system is between 6 and 8 where higher collision efficiency and stronger flocs were observed. $FeCl_3$ resulted in a larger ratio of the mass to volume of kaolin flocs (compactness) than those induced by ferrate which would facilitate the particle separation from water suspension through sedimentation process.

ACKNOWLEDGEMENTS

This work was supported by China Postdoctoral Science Foundation (Grant No. 2016M592271), 2016 Shandong Province Postdoctoral Innovation (Grant No. 201603007), Fundamental Research Funds for the Central Universities (Grant No. 18CX02106A), Shandong Provincial Natural Science Foundation (ZR2019MB022).

CONFLICT OF INTEREST

The authors declare no conflict of interest.

DATA AVAILABILITY STATEMENT

All relevant data are included in the paper or its Supplementary Information.

REFERENCES

Amirtharajah, A. & Melia, C. R. 1990 *Coagulation Processes: Destabilization, Mixing, and Flocculation in Water Quality and Treatment, FW Pontius*. McGraw-Hill, New York, NY, USA.

Benn, F., Fawell, P., Halewood, J., Austin, P., Costine, A., Jones, W., Francis, N., Druett, D. & Lester, D. 2018 Sedimentation and consolidation of different density aggregates formed by polymer-bridging flocculation. *Chemical Engineering Science* **184**, 111–125.

Bonanomi, E., Sefcik, J., Morari, M. & Morbidelli, M. 2004 Analysis and control of a turbulent coagulator. *Industrial & Engineering Chemistry Research* **43** (19), 6112–6124.

Bushell, G. C., Yan, Y. D., Woodfield, D., Raper, J. & Amal, R. 2002 On techniques for the measurement of the mass fractal dimension of aggregates. *Advances in Colloid and Interface Science* **95** (1), 1–50.

Callesen, I., Keck, H. & Andersen, T. J. 2018 Particle size distribution in soils and marine sediments by laser diffraction using Malvern Mastersizer 2000—method uncertainty including the effect of hydrogen peroxide pretreatment. *Journal of Soils and Sediments* **18** (7), 2500–2510.

Chassagne, C. & Safar, Z. 2020 Modelling flocculation: towards an integration in large-scale sediment transport models. *Marine Geology* **430**, 106361.

Cui, J., Zheng, L. & Deng, Y. 2018 Emergency water treatment with ferrate (VI) in response to natural disasters. *Environmental Science: Water Research & Technology* **4** (3), 359–368.

Duan, J. & Gregory, J. 2003 Coagulation by hydrolysing metal salts. *Advances in Colloid and Interface Science* **100**, 475–502.

Elimelech, M. J., Gregory, J., Jia, X. & Williams, R. A. 1995 *Particle Deposition and Aggregation: Measurement, Modeling, and Simulation*. Butterworth-Heinemann Ltd, Oxford, UK.

Goodwill, J. E., Jiang, Y., Reckhow, D. A., Gikonyo, J. & Tobiason, J. E. 2015 Characterization of particles from ferrate preoxidation. *Environmental Science & Technology* **49** (8), 4955–4962.

Goodwill, J. E., Jiang, Y., Reckhow, D. A. & Tobiason, J. E. 2016 Laboratory assessment of ferrate for drinking water treatment. *Journal-American Water Works Association* **108** (3), E164–EE74.

Graham, N., Khoi, T. & Jiang, J.-Q. 2010 Oxidation and coagulation of humic substances by potassium ferrate. *Water Science and Technology* **62** (4), 929–936.

Gregory, J. 2004 Monitoring floc formation and breakage. *Water Science and Technology* **50** (12), 163–170.

Hounslow, M. J., Ryall, R. L. & Marshall, V. R. 1988 A discretized population balance for nucleation, growth, and aggregation. *AICHE Journal* **34** (11), 1821–1832.

Hsu, J. W. C., Speers, R. A. & Paulson, A. T. 2001 Modeling of orthokinetic flocculation of *Saccharomyces cerevisiae*. *Biophysical Chemistry* **94** (1–2), 47–58.

Hubbe, M. A. 2005 Mechanistic aspects of microparticle systems. *TAPPI J.* **4** (11), 23–28.

Jiang, J., Lloyd, B. & Grigore, L. 2001 Disinfection and coagulation performance of potassium ferrate for potable water treatment. *Environmental Engineering Science* **18** (5), 323–328.

Kusters, K. A. 1991 *The Influence of Turbulence on Aggregation of Small Particles in Agitated Vessels*. PhD Dissertation/Thesis, Doctoral dissertation, Eindhoven University of Technology, The Netherlands.

Li, C., Li, X. & Graham, N. 2005 A study of the preparation and reactivity of potassium ferrate. *Chemosphere* **61** (4), 537–543.

Liu, L. S., Yang, G. L. & Yu, M. H. 2012 Simulation for sludge flocculation I: Brownian dynamic simulation for perikinetic flocculation of charged particle. *Mathematical Problems in Engineering* **2012**, 1–17.

Lv, D., Zheng, L., Zhang, H. & Deng, Y. 2018 Coagulation of colloidal particles with ferrate(VI). *Environmental Science: Water Research & Technology* **4** (5), 701–710.

Ma, J. & Liu, W. 2002a Effectiveness and mechanism of potassium ferrate (VI) preoxidation for algae removal by coagulation. *Water Research* **36** (4), 871–878.

Ma, J. & Liu, W. 2002b Effectiveness of ferrate (VI) preoxidation in enhancing the coagulation of surface waters. *Water Research* **36** (20), 4959–4962.

Prucek, R., Tuček, J. I., Kolařík, J., Filip, J., Marušák, Z. K., Sharma, V. K. & Zbořil, R. 2013 Ferrate (VI)-induced arsenite and arsenate removal by in situ structural incorporation into magnetic iron (III) oxide nanoparticles. *Environmental Science & Technology* **47** (7), 3283–3292.

Rau, M. J., Ackleson, S. G. & Smith, G. B. 2018 Effects of turbulent aggregation on clay floc breakup and implications for the oceanic environment. *PLoS One* **13** (12), e0207809.

Runkana, V., Somasundaran, P. & Kapur, P. C. 2006 A population balance model for flocculation of colloidal suspensions by polymer bridging. *Chemical Engineering Science* **61** (1), 182–191.

Saffman, P. G. & Turner, J. S. 1956 On the collision of drops in turbulent clouds. *Journal of Fluid Mechanics* **1** (1), 16–30.

Sang, Y. & Englezos, P. 2012 Flocculation of precipitated calcium carbonate (PCC) by cationic tapioca starch with different charge densities. I: experimental. *Colloids and Surfaces A: Physicochemical and Engineering Aspects* **414**, 512–519.

Sang, Y. & Xiao, H. 2008 Clay flocculation improved by cationic poly (vinyl alcohol)/anionic polymer dual-component system. *Journal of Colloid and Interface Science* **326** (2), 420–425.

Sang, Y. & Xiao, H. 2009 Preparation and application of cationic cellulose fibers modified by in situ grafting of cationic PVA. *Colloids and Surfaces A: Physicochemical and Engineering Aspects* **335** (1–3), 121–127.

Sharma, V. K., Zboril, R. & Varma, R. S. 2015 Ferrates: greener oxidants with multimodal action in water treatment technologies. *Accounts of Chemical Research* **48** (2), 182–191.

Shirazi, M., van de Ven, T. G. M. & Garnier, G. 2003 Adsorption of modified starches on pulp fibers. *Langmuir* **19** (26), 10835–10842.

Smith, D. K. W. & Kitchener, J. A. 1978 The strength of aggregates formed in flocculation. *Chemical Engineering Science* **33** (12), 1631–1636.

Spicer, P. T. & Pratsinis, S. E. 1996 Coagulation and fragmentation: universal steady-state particle-size distribution. *AICHE Journal* **42** (6), 1612–1620.

Teixeira, J. 1988 Small-angle scattering by fractal systems. *Journal of Applied Crystallography* **21**, 781–785.

Tien, K. T., Graham, N. & Jiang, J.-Q. 2008 *Evaluating the Coagulation Performance of Ferrate: A Preliminary Study*. ACS Publications, San Francisco, CA, USA.

Tran Tien, K. 2012 *Evaluation of Potassium Ferrate as a Coagulant in Water and Wastewater Treatment*. PhD Thesis, Imperial College London, UK.

Vik, E. A. & Eikebrokk, B. 1989 *Coagulation Process for Removal of Humic Substances From Drinking Water*. ACS Publications, Washington, DC, USA.

von Smoluchowski, M. V. 1917 Mathematical theory of the kinetics of the coagulation of colloidal solutions. *Zeitschriftfuer Physikalische Chemie* **92**, 129–168.

Wiesner, M. R. 1992 Kinetics of aggregate formation in rapid mix. *Water Research* **26** (3), 379–387.

Wilen, B. M., Jin, B. & Lant, P. 2003 Impacts of structural characteristics on activated sludge floc stability. *Water Research* **37** (15), 3632–3645.

Yeung, A. K. C. & Pelton, R. 1996 Micromechanics: a new approach to studying the strength and breakup of flocs. *Journal of Colloid and Interface Science* **184** (2), 579–585.

Yu, W., Yang, Y. & Graham, N. 2016 Evaluation of ferrate as a coagulant aid/oxidant pretreatment for mitigating submerged ultrafiltration membrane fouling in drinking water treatment. *Chemical Engineering Journal* **298**, 234–242.

Zheng, L. & Deng, Y. 2016 Settleability and characteristics of ferrate (VI)-induced particles in advanced wastewater treatment. *Water Research* **93**, 172–178.

Zhou, J., Zhao, Z., Liu, J., Peng, W., Peng, X., Han, Y. & Xiao, P. 2019 Removal of Microcystis aeruginosa and control of algal organic matters by potassium ferrate (VI) pre-oxidation enhanced Fe (II) coagulation. *Korean Journal of Chemical Engineering* **36** (10), 1587–1594.

First received 23 November 2020; accepted in revised form 7 April 2021. Available online 19 April 2021